# $^4$He adsorption on a $H_2$-plated $C_{20}$ molecular surface: The formation of helium buckyballs

Sungjin Park and Yongkyung Kwon*
*Division of Quantum Phases and Devices, School of Physics, Konkuk University, Seoul 143-701, Korea*
(Received 10 January 2014; published 9 April 2014)

We perform path-integral Monte Carlo calculations to study the adsorption of $^4$He atoms on a $H_2$-plated $C_{20}$ molecular surface. It is found that 32 $H_2$ molecules form a complete solid layer on $C_{20}$, where each $H_2$ molecule is located either above one of the 12 pentagon centers or above one of the 20 carbon atoms. The angular density profiles of the first $^4$He layer on the $(H_2)_{32}$-$C_{20}$ surface reveal different quantum states as the number of $^4$He atoms $N$ varies. Especially, the helium layer exhibits an icosidodecahedron structure for $N = 30$, where each $^4$He atom is located at one of the vertices of 20 corner-sharing triangles. While the $^4$He density peaks for $N = 60$ constitute a truncated icosahedron with 12 pentagonal and 20 hexagonal faces, the additional atoms beyond $N = 60$ are found to be placed at the hexagon centers of the truncated icosahedron to form a hexakis truncated icosahedron for $N = 80$. The superfluid response of the $^4$He layer at a temperature of $T = 0.6$ K is found to be completely quenched for $N = 30$ and to be significantly suppressed for $N = 60$ and 80, reflecting the formation of compact buckyball structures.

DOI: 10.1103/PhysRevE.89.042118 PACS number(s): 67.10.Fj, 67.25.dr, 67.25.dw, 61.46.Bc

## I. INTRODUCTION

A system of $^4$He atoms adsorbed on a substrate has been a test bed to study how reduced dimensionality or finite size affects physical properties of a quantum fluid in a confined geometry. While superfluid transition in a thin film of $^4$He on an extended flat substrate exhibited characteristics of a Kosterlitz-Thouless transition [1,2], the $^4$He atoms confined inside a nanopore were predicted to show the Luttinger liquid behavior as a one-dimensional quantum fluid [3]. Graphite, the most abundant carbon allotrope in nature, is known to be a strong substrate for $^4$He on which multiple distinct helium layers have been observed [4]. Similar layering structures of the $^4$He adatoms have been predicted on the surfaces of other carbon allotropes including carbon nanotubes [5] and graphene [6–9]. Through the interplay between the $^4$He-$^4$He interaction and the $^4$He-substrate interaction, these helium layers could manifest various quantum phases such as commensurate and incommensurate solids.

The $^4$He adsorption on the outer surface of a fullerene molecule was first studied using a spherically averaged isotropic $^4$He-fullerene potential, from which distinct layered structures of $^4$He atoms were predicted to form on the fullerene molecular surfaces as on graphite [10,11]. A series of recent path-integral Monte Carlo (PIMC) calculations based on anisotropic $^4$He-fullerene potentials, which allowed the investigation of the helium corrugations on fullerene surfaces, showed that the completed first $^4$He layer on a single fullerene would be in different quantum states depending on the size of a fullerene molecule, for example, a commensurate solid on $C_{20}$ [12], an inhomogeneous fluid on $C_{28}$ [13], and an incommensurate solid on $C_{60}$ [14]. Furthermore, while the $^4$He layer on $C_{20}$ showed nanoscale supersolidity near its completion [12], the helium monolayer on $C_{60}$ was predicted to undergo a commensurate-incommensurate (C-IC) solid transition as the number of $^4$He adatoms increased [14], a phenomenon akin to helium on graphite. This C-IC transition was also predicted from global optimization and path-integral molecular dynamics calculations of Calvo [15] for $C_{60}^+$-doped $^4$He clusters. On the other hand, recent mass spectroscopic measurements for $^4$He adsorbed on an isolated $C_{60}^+$ confirmed experimentally the existence of a commensurate solid state where each of 12 pentagons and 20 hexagons on the fullerene surface was occupied by a single $^4$He atom [16].

As discussed above, physical properties of the $^4$He adlayer on a fullerene molecule are expected to depend on the size of the molecule as well as on its surface corrugation. One can tune these factors, along with the strength of the surface binding potential, by plating the fullerene surface with other particles more strongly bound to a fullerene than $^4$He. We here consider a system of $^4$He atoms adsorbed on the $C_{20}$ molecular surface coated with a single layer of para-$H_2$ molecules. Para-$H_2$, hereafter simply $H_2$, is a spinless bosonic compound, which has been long considered as the best candidate to find superfluidity other than a system of helium isotopes of $^4$He or $^3$He. Unlike helium, however, bulk $H_2$ is solidified at low temperatures because of strong interparticle interaction before a condensation phenomena such as superfluidity takes place. Therefore some scientists have focused on a confined or a finite-sized system to find hydrogen superfluidity [17–19]. Motivated by this along with possible application for hydrogen storage, Turnbull and Boninsegni performed ground-state quantum Monte Carlo calculations for $H_2$ molecules adsorbed on the outer surface of a fullerene molecule, from which they predicted a transition from a commensurate to an incommensurate layer with the increase of the chemical potential from its equilibrium value but did not find any evidence for hydrogen superfluidity [20]. Recent high-resolution mass spectroscopic measurements for $(H_2)_N C_{60}^+$ revealed the formation of an energetically favorable commensurate phase for $N = 32$, where each face of a $C_{60}^+$ ion is covered by one $H_2$ molecule [21].

Some years ago, Ebey and Vilches reported thermodynamic measurements of monolayer $^4$He adsorbed on graphite plated with a few layers of $H_2$, which revealed a low-temperature and

*ykwon@konkuk.ac.kr

 

low-density region for gas-liquid coexistence and probable solidification at high helium densities [22]. The torsional oscillator measurements of Nyéki *et al*. showed finite superfluid response in the second $^4$He layer adsorbed on hydrogen-plated graphite but provided no evidence for superfluidity in the first helium layer [23,24]. Chan and his coworkers later showed that the thickness of the nonsuperfluid or inert $^4$He layer on a substrate increased monotonically with the strength of the $^4$He-substrate interaction and hence it could be reduced by plating strongly binding substrates with some inert gas atoms or hydrogen molecules [25,26].

Using the PIMC method, we here investigate structural and superfluid properties of the $^4$He monolayer adsorbed on $C_{20}$ plated with a single layer of $H_2$ molecules. It is found that the $^4$He layer shows various quantum states as the number of $^4$He adatoms $N$ varies. While $^4$He adatoms form clusters at low helium coverages, the helium layer is found to exhibit an icosidodecahedron structure for $N = 30$, where $^4$He atoms are located at the vertices of 20 corner-sharing triangles on the near-spherical surface of a $H_2$-plated $C_{20}$. More dense buckyball structures of truncated icosahedrons are found for $N = 60$ and 80, even though they are not as rigid as the $N = 30$ icosidodecahedron. The superfluid response of the $^4$He monolayer on the $H_2$-plated $C_{20}$ is also found to depend on its helium coverage; the superfluid fraction is negligible at low helium coverages but increases rapidly at $T = 0.6$ K as the helium coverage increases beyond $N = 40$. Significant suppression of superfluidity observed at $N = 60$ and 80 reflects the formation of the compact buckyball structures. The paper is organized as follows. Section II deals with the computational details including the description of the $^4$He-$C_{20}$ and the $H_2$-$C_{20}$ potentials. The PIMC results along with the related discussions are presented in Sec. III. We summarize our findings in Sec. IV.

## II. COMPUTATIONAL DETAILS

In this study, both $H_2$ molecules and $^4$He atoms are treated quantum mechanically while a $C_{20}$ molecule is fixed at the origin without rotation. This is justified by the fact that a $C_{20}$ molecule has much larger mass than $H_2$ or $^4$He. The $^4$He-$C_{20}$ ($H_2$-$C_{20}$) interaction is assumed to be a sum of the pair potentials between each of the 20 carbon atoms and a $^4$He atom (a $H_2$ molecule). For the $^4$He-C interatomic pair potential, we employ an isotropic 6-12 Lennard-Jones potential proposed by Carlos and Cole to fit the helium scattering data on graphite [27,28]. Our $H_2$-C pair potential is also of the 6-12 type, which was used by Levesque *et al*. [29] to describe the $H_2$-nanotube interaction in their study of hydrogen storage in carbon nanotubes. As noted in Ref. [12], these substrate potentials allow us to investigate $H_2$ and $^4$He corrugations on the $C_{20}$ molecular surface. While we use an empirical exp-6 potential proposed by van den Bergh and Schouten [30] for the $^4$He-$H_2$ interaction, the well-known Aziz potential [31] and the Silvera-Goldman potential [32] are used for the $^4$He-$^4$He interaction and the $H_2$-$H_2$ interaction, respectively.

In order to calculate thermodynamic properties of $^4$He-$H_2$-$C_{20}$ complexes, we here employ the PIMC method which is based on Feynman's original idea of mapping the path integrals of quantum particles onto classical polymers. In the discrete path-integral representation, the thermal density matrix at a low temperature, $T$, is written as a convolution of $M$ high-temperature density matrices with a time step of $\tau = (Mk_BT)^{-1}$. All pair potentials between the constituents are used to derive exact two-body density matrices at the high temperature $MT$ [33,34], which was found to provide an accurate description of all involved interactions with a time step of $\tau^{-1}/k_B = 80$ K. The multilevel Metropolis algorithm described in detail in Ref. [33] is used to sample permutations among $^4$He atoms or among $H_2$ molecules as well as their imaginary-time paths.

With the PIMC method, one can compute the superfluid fraction of a quantum fluid as a function of temperature. Both $H_2$ and $^4$He superfluidities in the $^4$He-$H_2$-$C_{20}$ complexes are computed using an area estimator [33]:

$$f_\alpha^s = \frac{4m^2\langle A_\alpha^2\rangle k_B T}{\hbar^2 I_\alpha^{\rm cl}}, \tag{1}$$

where $m$ is the mass of a $^4$He atom or a $H_2$ molecule, $I_\alpha^{\rm cl}$ is the classical moment of inertia, and $A_\alpha$ is the area of a Feynman path projected onto a plane perpendicular to the principal axis $\hat{x}_\alpha$. This estimator for the superfluid fraction has non-negligible values only when the sizes of exchange-coupled paths are comparable to the system size [33].

## III. PIMC RESULTS

With the $H_2$-$C_{20}$ potential described above, We first performed the PIMC calculations for $H_2$ molecules adsorbed on $C_{20}$. We found that the first hydrogen layer is completed with 32 $H_2$ molecules, whose angular and radial density distributions are shown in Figs. 1(a) and 1(b), respectively. One can see 32 distinct density peaks located at the angular positions corresponding to 12 pentagon centers ($P$ sites) and 20 carbon sites ($C$ sites) on the $C_{20}$ molecular surface. The same commensurate structure was also observed in the $^4$He monolayer on $C_{20}$. While the first $^4$He layer on $C_{20}$ was shown to exhibit the nanoscale supersolidity induced by mobile vacancies near its completion, we observed no superfluidity in the first $H_2$ layer on $C_{20}$, regardless of the number of $H_2$ molecules. This distinction between the $H_2$ and the $^4$He adlayers could be understood by the fact that the $H_2$-$C_{20}$ interaction has a potential barrier much higher than that of the $^4$He-$C_{20}$ interaction. Since the global minima of the $H_2$-$C_{20}$ potential are located in the directions of the $P$ sites and the $C$ sites involve only its saddle points, 12 $H_2$ molecules at the $P$ sites are expected to be more tightly bound to $C_{20}$ than 20 $H_2$ molecules at the $C$ sites. This is confirmed in Fig. 1(b), where the dotted (dot-dashed) line represents the radial density profile of $H_2$ molecules at the $P$ ($C$) sites. We note that the same icosahedral structure consisting of 32 $H_2$ molecules, a pentakis dodecahedron, was recently observed through high-resolution mass spectroscopic measurements for $H_2$ clusters doped by a single $C_{60}^+$ cation [21]. However, unlike the $(H_2)_{32}$-$C_{60}^+$ complex where each of 32 adsorption sites on the $C_{60}$ molecular surface, 12 pentagon centers and 20 hexagon centers, accommodates a single $H_2$ molecule, all 32 lattice sites on the surface of $C_{20}$ are not the adsorption sites predetermined by the substrate potential. This tells us that the

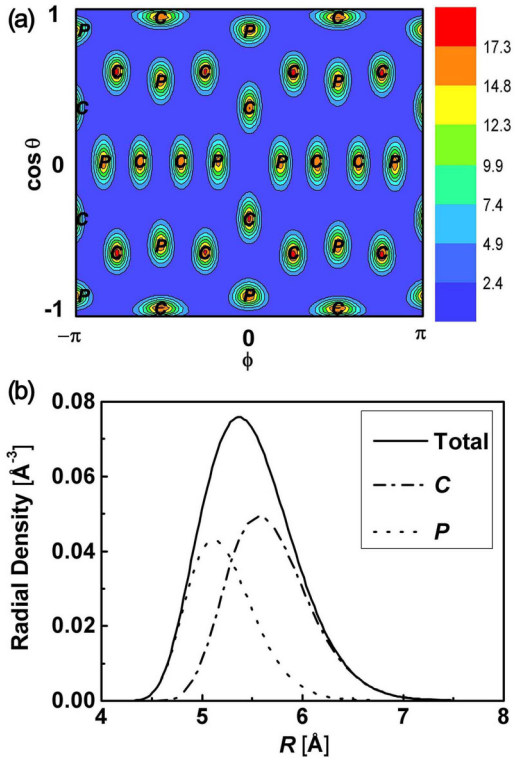


FIG. 1. (Color online) (a) Angular and (b) radial density distributions of 32 $H_2$ molecules adsorbed on $C_{20}$. The vertical axis and the horizontal axis in panel (a) correspond to the cosine of the polar angle $\theta$ and the azimuthal angle $\phi$ while the characters $C$ and $P$ represent the angular positions of the carbon atoms and those of the pentagon centers, respectively. The solid line in panel (b) represents the total density distribution and the dotted (dot-dashed) line corresponds to the density distribution of 12 (20) $H_2$ molecules located at the $P$ sites ($C$ sites).

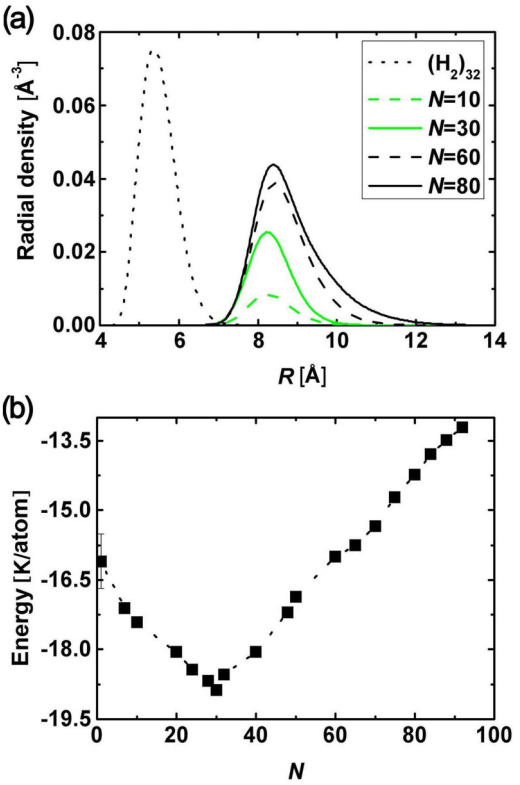


FIG. 2. (Color online) (a) Radial density distributions of 32 $H_2$ molecules (dotted line) and $N$ $^4$He atoms (solid and dashed lines) in the $(^4He)_N$-$(H_2)_{32}$-$C_{20}$ complex as a function of the distance from the center of $C_{20}$ and (b) the total energy per $^4$He atom of the $^4$He layer adsorbed on the $H_2$-plated $C_{20}$ surface in units of kelvin. The PIMC calculations were done at $T = 0.6$ K and the dotted line in panel (b) is just a guide to the eye.

$H_2$-$H_2$ interaction as well as the $H_2$-substrate interaction plays a crucial role in realizing this crystalline structure, shown in Fig. 1(a).

We now study the adsorption of $^4$He atoms on $C_{20}$ plated with 32 $H_2$ molecules. The radial density profiles of $H_2$ molecules (dotted line) and $^4$He atoms (solid and dashed lines) with respect to the $C_{20}$ molecular center are shown in Fig. 2(a) for different numbers of $^4$He adatoms $N$. The $^4$He density peaks are found to be located at a distance of $R \sim 8.2$ Å from the $C_{20}$ molecular center or ∼2.8 Å from the peak position of the $H_2$ density distribution. We note that the $H_2$ layer is well separated from the outer $^4$He layers with little overlap between them. This indicates that even with quantum fluctuations of both $^4$He and $H_2$ being fully incorporated in the PIMC calculations, $^4$He atoms cannot penetrate into the $H_2$ layer nor replace $H_2$ molecules from the immediate vicinity of $C_{20}$.

Figure 2(b) shows the energy per $^4$He atom of the first $^4$He layer adsorbed on the $H_2$-plated $C_{20}$ as a function of $N$, which was estimated by subtracting the energy of the $(H_2)_{32}$-$C_{20}$ complex from the total energy of the entire $(^4He)_N$-$(H_2)_{32}$-$C_{20}$ system. The binding energy of a single $^4$He atom to the $(H_2)_{32}$-$C_{20}$ complex is estimated to be $-16.1(6)$ K, which is close to the experimentally measured $^4$He binding energy ($16 \pm 2$ K) to liquid molecular hydrogen [35] as well as to a theoretical binding energy of 15.5 K [36] for a single $^4$He adatom on bulk solid $H_2$. As shown in Fig. 2(b), the energy per $^4$He atom decreases monotonically as the number of $^4$He atoms increases from $N = 1$ to $N = 30$ while it keeps increasing with the increase of the number of $^4$He atoms beyond $N = 30$. The lowest-energy configuration of the $^4$He layer, the most energetically stable state, occurs at $N = 30$. The decrease of the energy per particle with the increase of $N$ for $N < 30$ suggests that $^4$He atoms are congregated together to form clusters at low helium coverages, rather than fluids dispersed evenly over the near-spherical $H_2$-plated $C_{20}$ surface, because the $^4$He-substrate interaction is not strong enough to spread the $^4$He atoms throughout the surface. At high enough helium coverages beyond $N = 30$, these clusters are connected with each other to become homogeneous $^4$He films, which is reflected by the increase in the energy per particle for $N > 30$.

The structural properties of the $^4$He layer adsorbed on a $H_2$-preplated $C_{20}$ are now investigated by analyzing its angular density distributions, which are shown in Fig. 3 for different numbers of $^4$He adatoms $N$. For $N = 10$, the $^4$He angular density distribution shows that 10 $^4$He adatoms are not spread out over the whole spherical surface but are congregated in a limited region, confirming the cluster formation conjectured in the energetic analysis. One can see that the density peaks

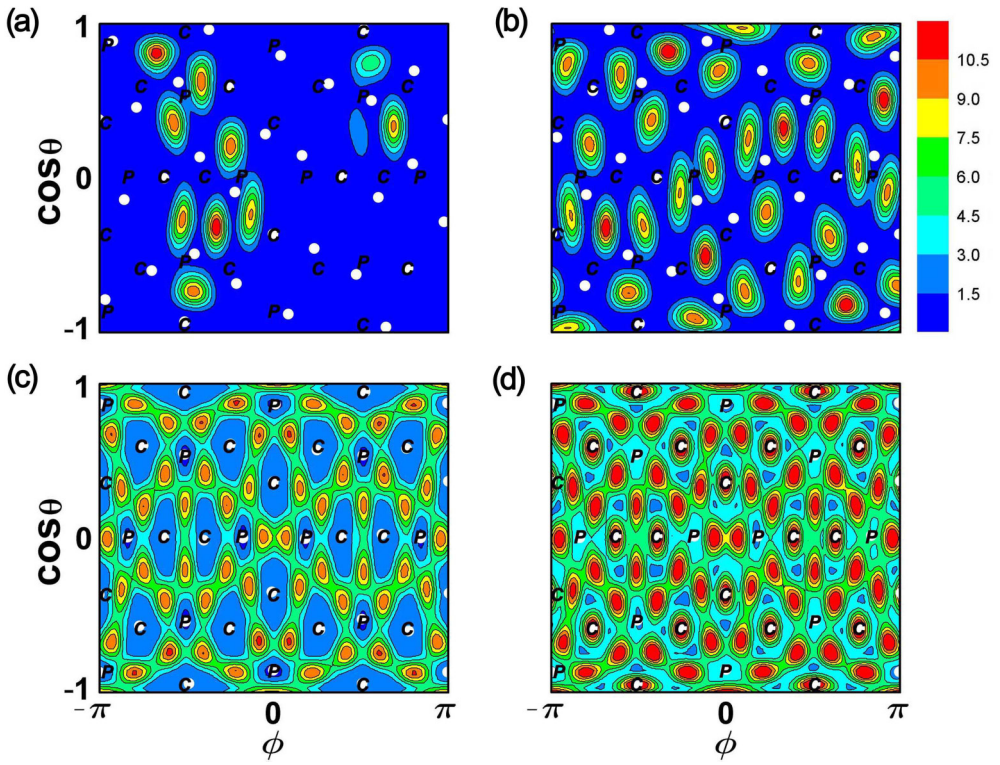


FIG. 3. (Color online) Contour plots of angular density distributions of $N$ $^4$He atoms adsorbed on the surface of an $(H_2)_{32}$-$C_{20}$ complex for (a) $N = 10$, (b) $N = 30$, (c) $N = 60$, and (d) $N = 80$. The horizontal axis corresponds to the azimuthal angle $\phi$ and the vertical one to the cosine of the polar angle $\theta$. The white dots represent the peak positions of the underlying $H_2$ layer and the characters $C$ and $P$ correspond to the angular positions of the carbon atoms and those of the pentagon centers of $C_{20}$, respectively. The PIMC calculations were performed at $T = 0.6$ K and all contour plots are in the same color scale denoted by the color table in the upper right-hand corner.

of 32 $H_2$ molecules are no longer located at the $C$ and $P$ sites [see the white dots in Fig. 3(a)], indicating that the uneven distribution of $^4$He atoms changes the structure of the underlying $H_2$ layer. Despite stronger binding of $H_2$ to $C_{20}$ than $^4$He, the underlying $H_2$ layer does not remain rigid during the $^4$He adsorption process, which reflects that some of the original lattice sites, i.e., $C$ sites, for 32 $H_2$ molecules are not potential minima of the $H_2$-$C_{20}$ interaction. For $N = 30$ where the helium adlayer has the lowest energy per $^4$He atom, one can observe 30 well-distinct density peaks constituting the vertices of 20 triangles on the spherical surface, each of which is centered at one of the underlying $H_2$ density peaks [see Fig. 3(b)]. The angular positions of the density peaks for $N = 30$ correspond to the vertices of an icosidodecahedron, an Archimedean solid whose surface consists of 12 pentagons and 20 corner-sharing triangles as shown in Fig. 4(a). As noted by Rousochatzakis *et al.* [37], this icosidodecahedron structure is a finite-size zero-dimensional realization of a planar Kagomé lattice on the spherical surface. A striking anomaly in the differential susceptibility observed recently in the giant Keplerate magnetic molecule of $Mo_{72}Fe_{30}$, which features 30 $Fe^{3+}$ ions on the vertices of an icosidodecahedron, was interpreted as a manifestation of frustrated antiferromagnetism due to the topological property of a polytope assembled with corner-sharing triangles [38]. From this we propose that a geometrically frustrated antiferromagnetism could be realized in the fermionic counterpart of this $^4$He layer, i.e., a $^3$He layer adsorbed on the $(H_2)_{32}$-$C_{20}$ complex.

As the number of $^4$He atoms increases beyond $N = 30$, the helium layer is found to go through fluid states consisting of delocalized $^4$He adatoms until another highly symmetric structure is observed at $N = 60$. Despite significant density overlap which is due to quantum fluctuations of $^4$He atoms including particle exchanges, one can clearly see 60 density peaks in the angular density distribution for $N = 60$ [see Fig. 3(c)]. The angular positions of these density peaks correspond to the vertices of a truncated icosahedron of Fig. 4(b) on the spherical surface, the same structure as a buckminsterfullerene of $C_{60}$. Each of 60 $^4$He density peaks is located at the center of a triangle consisting of three $H_2$ molecules, leading us to call this truncated icosahedron a

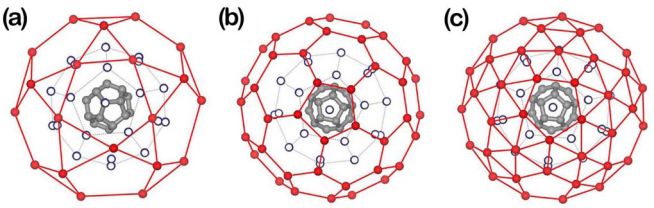


FIG. 4. (Color online) Three-dimensional plots of buckyball structures of $N$ $^4$He atoms [red (gray) solid dots] in the $(^4He)_N$-$(H_2)_{32}$-$C_{20}$ complexes for (a) $N = 30$ (icosidodecahedron), (b) $N = 60$ (truncated icosahedron), and (c) $N = 80$ (hexakis truncated icosahedron). The blue open dots and the gray-colored inner structure represent 32 $H_2$ molecules and a $C_{20}$ molecule, respectively.

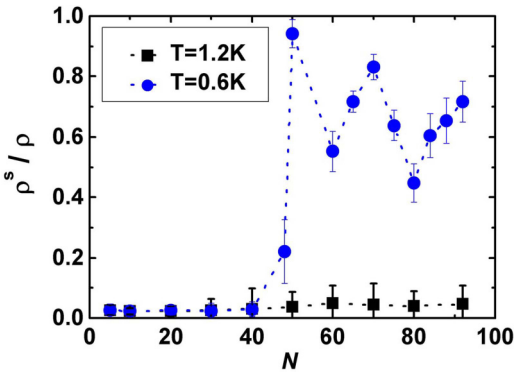


FIG. 5. (Color online) Superfluid fractions of the $^4$He layer on the surface of the $(H_2)_{32}$-$C_{20}$ complex as a function of the number of $^4$He atoms $N$ at $T = 0.6$ and 1.2 K. The dotted lines are just a guide to the eye.

$1 \times 1$ commensurate structure with respect to the underlying hydrogen layer. Noting that the same buckyball structure was not observed in the second $^4$He adlayer on top of the first $^4$He layer on $C_{20}$ [39], we conclude that the $H_2$-$^4$He interaction, which is stronger than the $^4$He-$^4$He interaction, plays a crucial role in realizing this icosahedral structure. In Fig. 3(d) for $N = 80$, one can find the additional density peaks located at the 20 hexagon centers of the truncated icosahedron structure. We call this structure, whose three-dimensional plot is shown in Fig. 4(c), a hexakis truncated icosahedron. Unlike the cases for $N \leqslant 30$, the underlying hydrogen layer for $N = 60$ and 80 preserves the pentakis dodecahedron structure commensurate with the $C_{20}$ molecular surface [see the white dots in Figs. 3(c) and 3(d)]. This tells us that as the $^4$He layer is filled with more $^4$He atoms, the density distribution of the outer $^4$He layer becomes more symmetric and does not disturb the structure of the inner $H_2$ layer. It is also found that the truncated icosahedron structures of Figs. 3(c) and 3(d) for $N = 60$ and 80 $^4$He atoms are more robust than the $N = 30$ icosidodecahedron structure of Fig. 3(b) against some defects in the underlying $H_2$ layer, i.e., when one $H_2$ molecule in the $H_2$ layer is replaced with a $^4$He atom.

We now analyze the relation between different structures of the $^4$He monolayer on the $H_2$-plated $C_{20}$ surface and its superfluid response. Figure 5 shows the superfluid fraction of the helium layer as a function of the number of $^4$He adatoms $N$, which were computed using the area estimator of Eq. (1). For $N \leqslant 40$, the superfluid fractions are negligible at both $T = 0.6$ and 1.2 K, suggesting that with a small number of $^4$He atoms, exchange coupling among $^4$He atoms takes place only locally and macroscopic exchanges spanning the whole spherical surface rarely, if ever, occur. This is consistent with the observation that the $^4$He atoms form clusters, rather than a homogeneous fluid, at low helium coverages. In addition, we note that for $N = 30$, where the helium atoms form an icosidodecahedron structure, the superfluid response is negligible. As the number of $^4$He adatoms increases beyond $N = 40$, one can observe a rapid increase of the superfluid fraction, reaching near the unit value for $N = 50$, at a temperature of $T = 0.6$ K while it remains negligible at $T = 1.2$ K. Though the superfluid fraction remains significant at $T = 0.6$ K with further increase of the number of $^4$He atoms beyond $N = 50$, one can see its noticeable suppression at $N = 60$ and 80. This suggests that the exchange couplings among $^4$He atoms are hindered in the compact icosahedron structures of Figs. 4(b) and 4(c) because of the decreased $^4$He mobilities.

## IV. CONCLUSIONS

From the PIMC calculations for the $(^4He)_N$-$(H_2)_{32}$-$C_{20}$ complexes, we have found that the $^4$He monolayer adsorbed on the $H_2$-plated $C_{20}$ molecular surface exhibits various quantum states as the number of $^4$He atoms $N$ changes. In particular, the structural analysis along with the energetic analysis showed that three different buckyball structures with the icosahedral symmetry could be realized in the $^4$He layer at low temperatures; the smallest buckyball structure of an icosidodecahedron, formed by 30 $^4$He atoms located at the vertices of 20 corner-sharing triangles, was found to be the lowest-energy state for the $^4$He layer while more dense helium buckyballs of truncated icosahedra were observed at $N = 60$ and 80. The icosidodecahedron structure, each of whose lattice points is shared by two neighboring triangles, is a zero-dimensional realization of a planar Kagomé lattice on the spherical surface. The angular density distributions whose peaks are well connected through the density overlap, especially for $N = 60$ and 80, reflect that these helium buckyballs are bound through weak van der Waals interaction and are not as rigid as a fullerene molecule consisting of covalent-bonded carbon atoms. Significant superfluid fractions observed at $T = 0.6$ K for $N = 60$ and 80, *albeit* being suppressed noticeably from the unit value, indicate prevalent exchange couplings among $^4$He atoms constituting these buckyballs. These lead us to conclude that the polyhedron structures exhibited by $N = 30$, 60, and 80 $^4$He adatoms on a $H_2$-plated $C_{20}$ are *quantum buckyballs*. Finally we conjecture that a geometrically frustrated antiferromagnetism could be realized in the icosidodecahedron structure consisting of 30 fermionic $^3$He atoms adsorbed on a $H_2$-plated $C_{20}$.

## ACKNOWLEDGMENTS

This work was supported by the Basic Science Research Program (Grant No. 2012R1A1A2006887) through the National Research Foundation of Korea funded by the Ministry of Education, Science and Technology.

[1] D. J. Bishop and J. D. Reppy, Phys. Rev. Lett. **40**, 1727 (1978).
[2] G. Agnolet, D. F. McQueeney, and J. D. Reppy, Phys. Rev. B **39**, 8934 (1989).
[3] A. Del Maestro, M. Boninsegni, and I. Affleck, Phys. Rev. Lett. **106**, 105303 (2011).
[4] G. Zimmerli, G. Mistura, and M. H. W. Chan, Phys. Rev. Lett. **68**, 60 (1992).

[5] M. C. Gordillo, Phys. Rev. Lett. **101**, 046102 (2008).
[6] M. C. Gordillo and J. Boronat, Phys. Rev. Lett. **102**, 085303 (2009).
[7] Y. Kwon and D. M. Ceperley, Phys. Rev. B **85**, 224501 (2012).
[8] M. C. Gordillo and J. Boronat, Phys. Rev. B **85**, 195457 (2012).
[9] J. Happacher, P. Corboz, M. Boninsegni, and L. Pollet, Phys. Rev. B **87**, 094514 (2013).
[10] E. S. Hernandez, M. W. Cole, and M. Boninsegni, Phys. Rev. B **68**, 125418 (2003).
[11] L. Szybisz and I. Urrutia, J. Low Temp. Phys. **134**, 1079 (2004).
[12] Y. Kwon and H. Shin, Phys. Rev. B **82**, 172506 (2010).
[13] B. Kim and Y. Kwon, J. Low Temp. Phys. **171**, 599 (2013).
[14] H. Shin and Y. Kwon, J. Chem. Phys. **136**, 064514 (2012).
[15] F. Calvo, Phys. Rev. B **85**, 060502(R) (2012).
[16] C. Leidlmair, Y. Wang, P. Bartl, H. Schöbel, S. Denifl, M. Probst, M. Alcamí, F. Martín, H. Zettergren, K. Hansen, O. Echt, and P. Scheier, Phys. Rev. Lett. **108**, 076101 (2012).
[17] P. Sindzingre, D. M. Ceperley, and M. L. Klein, Phys. Rev. Lett. **67**, 1871 (1991).
[18] S. Grebenev, B. Sartakov, J. P. Toennies, and A. F. Vilesov, Science **289**, 1532 (2000).
[19] Y. Kwon and K. B. Whaley, Phys. Rev. Lett. **89**, 273401 (2002).
[20] J. D. Turnbull and M. Boninsegni, Phys. Rev. B **71**, 205421 (2005).
[21] A. Kaiser, C. Leidlmair, P. Bartl, S. Zöttl, S. Denifl, A. Mauracher, M. Probst, P. Scheier, and O. Echt, J. Chem. Phys. **138**, 074311 (2013).
[22] P. S. Ebey and O. E. Vilches, J. Low Temp. Phys. **101**, 469 (1995).
[23] J. Nyéki, R. Ray, G. Sheshin, V. Maidanov, V. Mikheev, B. Cowan, and J. Saunders, Low Temp. Phys. **23**, 379 (1997).
[24] J. Nyéki, R. Ray, B. Cowan, and J. Saunders, Phys. Rev. Lett. **81**, 152 (1998).
[25] D. Tulimieri, N. Mulders, and M. H. W. Chan, J. Low Temp. Phys. **110**, 609 (1998).
[26] G. A. Csáthy and M. H. W. Chan, J. Low Temp. Phys. **121**, 451 (2000).
[27] W. E. Carlos and M. W. Cole, Surf. Sci. **91**, 339 (1980).
[28] M. W. Cole and J. R. Klein, Surf. Sci. **124**, 547 (1983).
[29] D. Levesque, A. Gicquel, F. L. Darkrim, and S. B. Kayiran, J. Phys.: Condens. Matter **14**, 9285 (2002).
[30] L. C. van den Bergh and J. A. Schouten, J. Chem. Phys. **89**, 2336 (1988).
[31] R. A. Aziz, M. J. Slaman, A. Koide, A. R. Allnatt, and W. J. Meath, Mol. Phys. **77**, 321 (1992).
[32] I. F. Silvera and V. V. Goldman, J. Chem. Phys. **69**, 4209 (1978).
[33] D. M. Ceperley, Rev. Mod. Phys. **67**, 279 (1995).
[34] R. E. Zillich, F. Paesani, Y. Kwon, and K. B. Whaley, J. Chem. Phys. **123**, 114301 (2005).
[35] C. G. Paine and G. M. Seidel, Phys. Rev. B **46**, 1043 (1992).
[36] L. Pierre, H. Guignes, and C. Lhuillier, J. Chem. Phys. **82**, 496 (1985).
[37] I. Rousochatzakis, A. M. Läuchli, and F. Mila, Phys. Rev. B **77**, 094420 (2008).
[38] C. Schröder, H. Nojiri, J. Schnack, P. Hage, M. Luban, and P. Kögerler, Phys. Rev. Lett. **94**, 017205 (2005).
[39] H. Shin and Y. Kwon, J. Korean Phys. Soc. **60**, 14 (2012).